Dry Metal Forming Open Access Journal

Fast Manuscript Track

Edited by Frank Vollertsen
Available online at elib.suub.uni-bremen.de

www.drymetalforming.de

Dry Met. Forming OAJ FMT 2 (2016) 025–039
Received 14 April 2016; published 09 May 2016

Tailored modifications of amorphous carbon based coatings for dry deep drawing

Marion Merklein[1], Michael Schmidt[2], Stephan Tremmel[3], Kolja Andreas[1], Tom Häfner[2], Rong Zhao[3]*, Jennifer Steiner[1]

[1]Institute of Manufacturing Technology, Friedrich-Alexander-Universität Erlangen-Nürnberg, Egerlandstr. 13, 91058 Erlangen, Germany
[2]Institute of Photonic Technologies, Friedrich-Alexander-Universität Erlangen-Nürnberg, Konrad-Zuse-Str. 3/5, 91052 Erlangen, Germany
[3]Institute of Engineering Design, Friedrich-Alexander-Universität Erlangen-Nürnberg, Martensstr. 9, 91058 Erlangen, Germany

Abstract

Avoiding negative effects of conventional lubrication in forming operations stimulates research on lubricant-free sheet metal forming. Without lubricants, the direct contact between tool and workpiece leads to intensive interaction in terms of increasing friction and wear. Especially, when forming aluminum alloys, adhesion is detected as main wear mechanism propagating already at the initial contact between tool steel and sheet material. Thus, surface modifications need to be developed to substitute the functions of conventional lubricants. Former studies revealed that amorphous carbon based coatings improved the tribological conditions. Depending on the specific coating type adhesion and friction could be significantly reduced. Besides achieving a lower level of friction, a control of material flow is necessary to improve the forming results in deep drawing processes. Thus, there is a need for contact zones with higher and lower friction to locally accelerate or restrict the flow of the sheet material. In order to achieve these tailored tribological conditions a broad range of surface modifications needs to be developed and evaluated in a process-like environment. The tribological behavior is affected by coating properties and structure. By varying gas flow and ratio for a-C:H coatings the relationship between deposition parameters and coating properties are investigated. A further approach to realize a broader range of friction coefficients is the laser based texturing of coated tools. Additionally, a laser based heat treatment is investigated to control the sp^2/sp^3 ratio of ta-C coatings to affect friction and wear mechanisms. The tribological behavior of the investigated surface modifications is analyzed in ring-on-disc and flat strip drawing tests. A surface characterization is performed to identify about the wear mechanisms. Based on the modifications of a-C:H and ta-C coatings a correlation between chemical and mechanical properties and the tribological behavior in contact with zinc-coated deep drawing steel and aluminum alloys is found.

Keywords: Dry Deep Drawing, Tribology, Carbon Based Coatings, Laser Based Modification

1 Introduction

The realization of lubricant-free deep drawing processes is motivated by ecological and economical aspects [1]. In conventional deep drawing operations, the workpiece is lubricated before forming and is cleaned and dried afterwards. The cleaning and drying steps are necessary before further production steps like joining or coating can follow. Customary lubricants as well as cleaning agents often contain environmental harmful materials like chloroparaffins [2] and aqueous alkaline type detergents [3], respectively. Eliminating the lubrication would lead to a shorter process chain as well as prevent the waste of non-renewable and ecologically hazardous substances. Beside these advantages, dry deep drawing faces several challenges due to increased friction and distinctive wear. The vision of the project ‘Lubricant free forming with tailored tribological conditions’ within the priority program SPP1676 is the realization of a dry deep drawing process with the help of a tailored tool with locally adapted tribological conditions. Different types of surface modifications are evaluated to generate tailored tribological properties. One approach to reduce friction under dry conditions is the application of coatings. Especially, carbon based coatings are known for their positive influence on friction reduction and high wear resistance [4]. Within this research project tetrahedral amorphous (ta-C) and hydrogenated amorphous carbon based coatings with and without tungsten modification (a-C:H:W, a-C:H) are

© 2016 The Authors. Selection under responsibility of BIAS - Bremer Institut für angewandte Strahltechnik GmbH.
*E-mail address of corresponding author: zhao@mfk.fau.de

investigated. As sheet materials the commonly used mild deep drawing steel DC04 and two aluminum alloys (AA6014, AA5182) are selected. Former studies within this research project compared the tribological conditions of lubricated and lubricant-free sliding contacts. These tests showed that the friction increased from a level of 0.03 to 0.05 with lubrication up to 0.6 without lubricants depending on the sheet material. This elevated friction is correlated with immediate adhesion. Thus, the aim of surface modifications is to prevent adhesive wear and reduce friction to the range of lubricated conditions. Strip drawing tests were performed to identify the potential of several carbon based coating systems Fig. 1 summarizes the resulting dry friction coefficients for the three different coatings types compared to the tests with uncoated tools. The surfaces of all coated tools were polished or brushed after depositions process to reduce amount and height of roughness asperities. Comparing the different coating types a broad range of friction coefficients is determined.

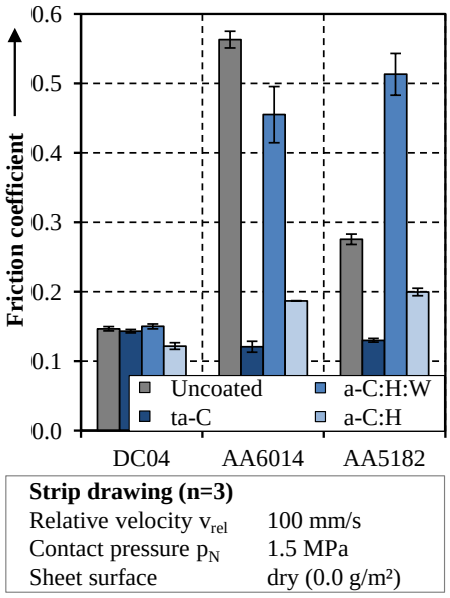

Fig. 1: Friction coefficients determined in dry strip drawing tests for varying coating types

Tools with a-C:H:W coatings reveal an insufficient tribological behavior especially in contact with both aluminum alloys. Only slight friction reduction is achieved for AA6014 and even higher friction compared to the uncoated case results for AA5182. For both sheet materials adhesion caused distinctive wear on the tools already after the first strip. Thus, the analyzed a-C:H:W coatings are inappropriate for lubricant-free forming and are not investigated within this study. In order to improve the tribological conditions an a-C:H top layer was deposited on an a-C:H:W base coating. Strip drawing tests with a-C:H coatings revealed a promising influence on friction and wear for DC04 and both aluminum alloys as shown in Fig. 1. Therefore, the development of a-C:H coatings is further analyzed in this paper. Tools with ta-C coatings lead to relatively low friction coefficients in contact with the investigated sheet materials. Thus, the applied ta-C variant seems promising for dry deep drawing of DC04 and both aluminum alloys.

Previous results of this research project as shown in Fig. 1 revealed different predominating tribological behavior of aluminum alloys and deep drawing steels in dry contact. AA5182 and AA6014 have a generally high adhesion tendency. Thus, the main focus of surface modifications for aluminum alloys is the prevention of adhesive wear. In contrast, for DC04 independent of the analyzed surface coating no adhesion occurred. As wear mechanism abrasion of zinc particles was observed in former investigations. Due to these diverse dominating tribological mechanisms different approaches for realization of dry deep drawing are necessary depending on the sheet material. The approaches analyzed in this investigation are summarized in Fig. 2. For both aluminum alloys ta-C coatings already achieve promising results in terms of low friction (Fig. 1) and prevention of immediate adhesion as shown in [5].

With a-C:H coatings adhesion could be reduced to a microscopic scale and friction was reduced to about 0.2 (Fig. 1). This investigation focusses on the further development of a-C:H coatings in dry contact with aluminum alloys to evaluate if the same or even better tribological behavior can be achieved compared to ta-C. As the a-C:H coatings show lower residual stresses and thus, higher adhesion strength [6], they might show longer life-time compared to ta-C coatings. Furthermore, the conventional PECVD based deposition process of smooth a-C:H coatings represents a cheaper process compared to the ta-C deposition, which is necessarily supported by magnetic filtering during cathodic vacuum arc process to generate smooth surfaces.

The methodology in Fig. 2 shows the approach for developing a-C:H coatings. Coatings with different chemical and mechanical properties are deposited by varying parameters of the deposition process. A characterization of coating properties and tribological behavior is performed to correlate deposition parameters and coating characteristics. In a first step, the tribological behavior is analyzed in tribometer tests. Future studies will be conducted by strip drawing tests to analyze the transferability to an open tribological system. For DC04 the tribological investigations focus on the control of the material flow and trapping of abrasive zinc particles. Laser based processing of coatings was selected to achieve these scopes. As coating variant the approved ta-C coating type was selected for first investigations because this coating variant showed promising tribological properties independent of the sheet material. This will facilitate the transferability of the results with DC04 to AA6014 and AA5182 in future studies. Furthermore, a broader range of variation of laser based heat treatment is possible due to the higher sp^3 content of ta-C. The material flow during deep drawing will be achieved with locally varied friction conditions. Therefore, surface modifications which increase friction but at the same time do not lead to higher wear are necessary. One approach for local adapted friction is the heat treatment of ta-C coatings to achieve a local increased friction by

influencing the graphitization ratio of sp^2 and sp^3 hybridized atoms. The chemical properties are adapted by varying the sp^2/sp^3 ratio. In a first step, the tribological behavior is analyzed in tribometer tests. Strip drawing tests will be conducted in future investigations to analyze the mechanisms under more process-like conditions. In order to trap abrasive zinc particles and further improve the material flow micro features are applied on ta-C coatings. Former investigations revealed that micro features on carbon based coatings could trap wear particles and increase friction in a closed tribological system depending on the feature geometry [7]. In this study, depth and area coverage of the features are varied to analyze the tribological mechanisms. In tribometer tests abrasive particles partially remain in the contact zone and thus distort the tribological results. Therefore, in this investigation all tribological tests with textured ta-C tools are conducted directly in strip drawing tests. After understanding the tribological mechanisms the results regarding control of material flow can be adapted for tribological systems with aluminum alloys in future studies.

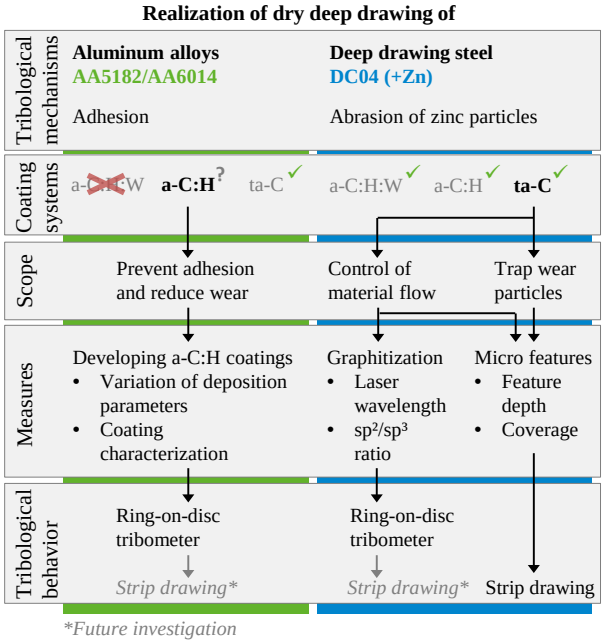

Fig. 2: Methodology of current investigation

2 Laboratory test setups and characterization methods

2.1 Tribological characterization

The tribological behavior was investigated in tribometer and strip drawing tests. All experiments were conducted under lubricant-free conditions. Therefore, the tool and workpiece surfaces were cleaned before testing with isopropanol. For tribometer test the ring-on-disc configuration (Wazau, TRM 1000) was used. The tests were conducted under ambient atmosphere with relative humidity RH = 43 % ± 2.4 % at room temperature (T = 23.2 ± 0.4 °C). The tribological system consists of a unidirectional rotating ring and a fixed square specimen made of sheet material (28 x 28 x 1 mm). The ring with coating or laser modified feature was pressed against the examined sheet material with a defined normal force. Both ring and sheet are arranged vertically, the rotating ring being positioned above. The friction coefficient μ_{rod} is expressed using the torque coefficient. The active torque is registered by a torque shaft and the reactive frictional torque is measured by a torque module. The experiment was repeated three times for each surface modification/sheet pair. The detailed tribometer setup is described in Fig. 3. The applied ring-on-disc tribological system is a closed tribological system in which the ring and disc are permanent parts of the system beyond the duration of loading, and constantly participate in the tribological process [8]. Thus, there is a stronger flattening of the sheet surface which might reduce the resistance towards sliding over the sliding length. Additionally, heating effects, accumulative adhesion and loose wear particles influence the tribological conditions in a closed system.

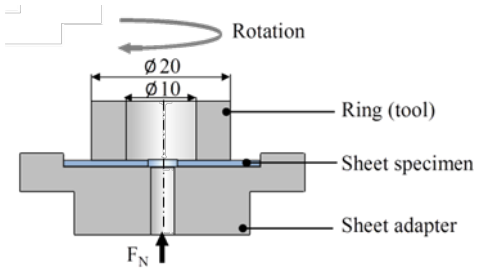

Fig. 3: Setup of the ring-on-disc tribometer

Due to the drawbacks of the closed ring-on-disc tribometer an open tribological system is additionally used to investigate the tribological behavior. Strip drawing tests were selected to determine friction coefficients in an environment closer to real forming processes. The flat strip drawing test (Fig. 4) models the tribological conditions of the flange area of a deep drawing process. A sheet metal strip is located between an upper fixed and a lower movable friction jaw which applies a defined normal force. Within this study, the contact pressure was varied between 4.5 and 9.0 MPa depending on the friction jaw properties. Under real forming conditions the pressure in the flange area is selected in a range from 1 up to 10 MPa. During drawing of the strip the necessary drawing force is recorded. By applying the Coulomb friction law the friction coefficient μ is determined as relation of drawing force to normal force. The friction jaws measure 100 x 55 mm. To ensure that the cutting edge is not in contact with the tools, the sheet metal strips have a width of 65 mm.

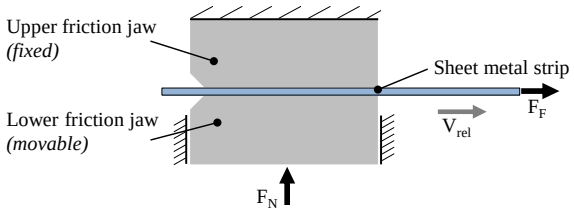

Fig. 4: Principle of flat strip drawing test

2.2 Coating characterization

After deposition, the a-C:H coating surfaces were analyzed using a laser scanning microscope (LSM; Keyence, VK-X 100K). The average distance between the highest peak and lowest valley R_z and the reduced peak height R_{pk} were characterized by tactile stylus measurements according to DIN EN ISO 4287 [9]. The measurements were repeated five times per coating variant. The interfacial adhesions between the coating and the substrate were measured by scratch tests according to DIN EN 1071-3 [10]. Using an optical microscope the normal force L_{c1}, at which the first failure of the coating occurs, was evaluated. The crater grinder method was applied to measure the coating thickness according to DIN EN 1071-2 [10]. The measurements of critical force and coating thickness were repeated three times on coated polished disc per coating variant, to ensure measurements with small standard deviations. Micro hardness of 10 points of the coated surfaces was determined by Vickers indentation (Fischer, FISCHERSCOPE H2000) with indentation force of 10 mN in 10 s according to DIN EN ISO 14577-1 [11].

Chemical coating properties were analyzed using Raman spectroscopy. The Raman spectroscopy measures the inelastic scattering of chemical bonds by laser. Raman spectra were acquired from all the coating samples to investigate their chemical bond configurations. The Raman analysis was conducted in the range of 800 to 2000 cm^{-1} since all carbon coatings show their characteristic peaks in this range [12]. The applied Raman model is equipped with a CCD detector with Nd:YAG laser at 532 nm. The applied laser power was 10 mW to avoid undesired structure changes or even damage of the coating [13].

3 Development of surface modifications

3.1 a-C:H coatings

From the results of previous works [7], [14], adhesion is considered as the dominating wear mechanism in dry contact with aluminum. For a systematic investigation of an a-C:H coatings for dry forming tools, a pre-evaluation of possible parameters which affect the coating properties was conducted. As shown in Fig. 5, many factors can affect the final features of an a-C:H coating and its tribological performance, which cover from precursor gas species, existence of sputter gas, gas pressure, substrate bias voltage, reactor temperature, to previous etching, heating processes and even contaminations in the reactor. This parameters affect the coating properties differently which will be discussed in details in the next paragraph. The divers coating properties have direct or indirect impacts on wear mechanisms and influence the friction conditions. The friction conditions affect the wear behavior, like loose particle occurrence and adhesion accumulation between tool and workpiece. In order to improve the friction conditions against aluminum alloys a-C:H coatings are applied on tool surface. Due to the great impact of the chemical structure of amorphous carbon coatings on the tribological behavior the precursor gas, process pressure and sputter gas will be systematically investigated. The substrate bias voltage was kept constant at a middle level due to its contribution of a high compressive stress.

The substrate bias voltage U_{bias} is well known to have great impact on coating growth structure and hardness [15]. Under high substrate bias U_{bias} the charged atoms or particles in the reactor can obtain high kinetic energy and thus high hardness as well as dense structure. With increasing atomic energy the compressive stress rises quickly and reaches its maximum if the impact energy is 20 eV per atom [16]. Furthermore, frequently bombardment leads also to great uncontrolled thermal effect to the substrates, e.g. a deposition process with substrate bias of -1,200 V leads to substrate self-heating to 160-170 °C, without any external heating system. An available process window of bias voltage varies from -400 to -550 V. The bias voltage higher than -550 V produced only dust on the polished disc substrates. In contrast, the plasma get not ignited at U_{bias} lower than -400 V. The investigated substrate bias voltage U_{bias} was kept constant at -550 V. This value is chosen to ensure the formation of a consistent a-C:H coating system with acceptable adhesion and high hardness.

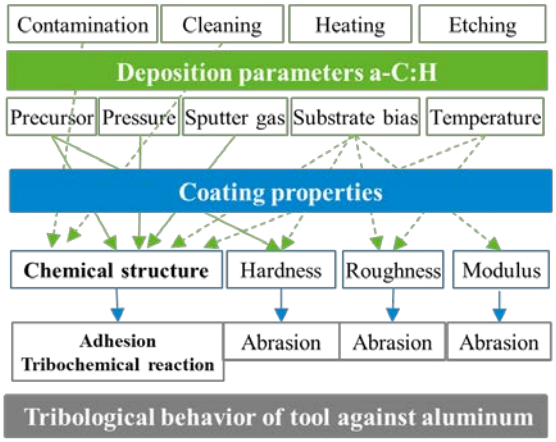

Fig. 5: Development of a-C:H coatings for dry metal forming tool for aluminum alloys.

In general a-C:H coatings can be deposited at temperatures from room temperature [17] to higher than 1000 °C according to different techniques. Low temperatures improve formation of the sp^3 bonds, density and compressive stress of a-C:H coatings [18],[19]. Considering the self-heating effect at the selected U_{bias} the lowest achievable temperature is 80°C.

The investigated a-C:H coatings were deposited using a hybrid PVD/PECVD coating machine (H-O-T, TT 300) with a twofold rotating charging rack. The basic coating system consists of a Cr adhesive layer, a WC interlayer, an a-C:H:W interlayer and the a-C:H functional layer. This coating architecture was chosen to ensure a sufficient adhesion of the a-C:H coating to the steel substrate. For the Cr adhesive layer and the WC interlayer arc evaporation and unbalanced magnetron sputtering were used as coating technologies,

respectively. The a-C:H coating functional layer was deposited by PECVD using C_2H_2 as precursor gas. A coating thickness of the a-C:H functional layer of around 2 µm is intended. The deposition time for all a-C:H functional layers were kept constant to 8 580 s according to the deposition rate of a similar a-C:H coating system reported in [14]. The admissible C_2H_2 and Ar gas flows in the reactor are 20-290 sccm and 0-500 sccm, respectively. The lowest total gas flow to initiate the glow discharge in a reactor of 300 l is about 200 sccm using mid frequency power supply (40 kHz, pulse width 5 µs). A series of a-C:H coatings deposited under gas ratios of $\Phi(Ar)/\Phi(Ar+C_2H_2)$ from 0 to 70 % were investigated in [20]. Coatings which were deposited in the range of $\Phi(Ar)/\Phi(Ar+C_2H_2) = 10$ to 50 % showed generally linear relationships between gas ratio and essential coating properties like coating roughness, wear rate, compressive stress or elastic modulus. If the gas mixture is further diluted with Ar the tendencies of some coating properties associated with gas ratios would be changed, e.g. coating compressive stress increases with Ar dilution and reached its maximum if $\Phi(Ar)/\Phi(Ar+C_2H_2) = 50$ %; wear rate reached its minimum if $\Phi(Ar)/\Phi(Ar+C_2H_2) = 50$ %.

In this work, the a-C:H coatings were deposited on tool steel 1.2379 (X155CrVMo12). Prior to coating process, the substrates were hardened to HRC 60 ± 1. Measurements of the coating properties were conducted on coating samples deposited on polished disc-shaped (Ø25 x 5 mm) substrate. The applied disc-shaped substrates were polished to $R_z \leqslant 0.2$ µm and $R_{pk} \leqslant 0.01$ µm to ensure a better sample preparation. After determining the coating thickness the coated disc surfaces were additionally after-treated to ensure smaller standard deviations, especially for the hardness determination considering Bückle rule [11]. The coating samples for tribological tests were deposited on ring-shaped substrates with inner and outer diameter of 10 and 20 mm, respectively. The ring-shaped substrate surfaces were lapped and polished to a roughness of $R_z = 0.9 \pm 0.1$ µm and $R_{pk} = 0.1 \pm 0.01$µm which represents the surface quality of conventional deep drawing tools. Prior to tribological tests, the coated surfaces were polished using 1 µm diamond suspension to remove increased surface asperities.

The gas flow ratios were varied in the range of $\Phi(C_2H_2)/\Phi(Ar) = 17$ to 50 % to prepare coatings with different mechanical properties. The detailed deposition parameters are shown in Tab.1.

Tab. 1: Variation of C_2H_2 and Ar flows for deposition of the a-C:H coatings

Sample ID	$\Phi(C_2H_2)$	Φ(Ar)	$\Phi(C_2H_2)/\Phi$(Ar)	$\Phi(Ar+C_2H_2)$
	sccm	*sccm*		*sccm*
100/100	100	100	1:1	200
150/150	150	150	1:1	300
161/64	161	64	2.5:1	225
188/62	188	62	3:1	250
166/34	166	34	5:1	200
220/40	220	40	5.5:1	260
250/50	250	50	5:1	300

The total thicknesses of the generated coating systems including interlayers are in the range of 1.5 µm to 3.0 µm. The Cr, WC and a-C:H:W interlayers have a constant total thickness of around 0.37 µm according to a similar coating system with the same interlayers in [14]. The thickness measurements were conducted on original deposited steel disc without polishing. The critical loads for the first crack are in the range of 12 N-18 N. Detailed values are summarized in Tab. 2.

Tab. 2: Coating properties of all a-C:H variations, n = 3.

Coating	Thickness	Adhesion
	t in µm	L_{c1} in N
100/100	1.65±0.07	14.0±2.0
150/150	2.19±0.17	15.0±2.0
161/64	1.77±0.22	15.0±1.0
188/62	2.24±0.10	16.0±2.0
166/34	1.51±0.12	12.0±1.0
220/40	2.34±0.07	18.5±1.0
250/50	2.96±0.08	16.3±0.6

The hardness and indentation values of each sample were summarized in Tab. 3.

Tab. 3: Mechanical properties of all a-C:H variations, n = 10.

Coating	Hardness	Indentation modulus
	HV 0.001	E_{IT} in GPa
100/100	2 087.0±25.2	555.1±11.3
150/150	1 883.6±187.7	461.5±62.3
161/64	2 284.8±129.4	606.8±39.9
188/62	2 031.5±110.1	531.6±26.8
166/34	2 202.3±92.8	589.3±24.0
220/40	1 936.8±109.5	502.7±28.9
250/50	1 922.9±117.4	475.7±30.0
Tool steel, hardened	642.8±88.2	164.6±16.7

Fig. 6 shows LSM images of a representative a-C:H coated surface before and after mechanical after-treatment. Fig. 6a) depicts that surface asperities due to small particles with height up to 1 µm are distributed on the surface. They result from a large number of macro-particles (the so-called “droplets”) entrapped in the Cr adhesive layer. As shown in Fig. 6b), after polishing the particles on coating surfaces were removed. The roughness of coated rings after coating process varies from $R_z = 1.3$ µm–1.6 µm and $R_{pk} = 0.29$ µm–0.36 µm. The coating samples are mechanical polished for tribological tests. Due to varied hardness of the coating samples the surface quality after polishing varied between $R_z = 0.5$ µm-0.7 µm and $R_{pk} = 0.05$ µm-0.07 µm.

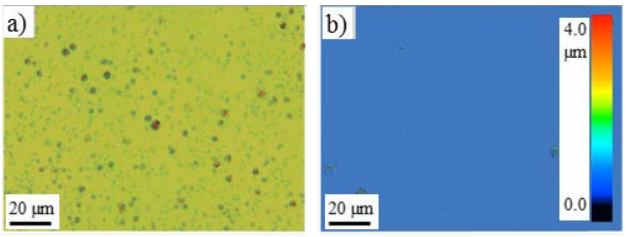

Fig. 6: LSM images of a-C:H coating 220/40 surface topography a) before and b) after polishing

The uncoated tool steel rings for reference tests were polished to a comparable R_{pk} value as the coating samples. The detailed values are summarized in Fig. 7.

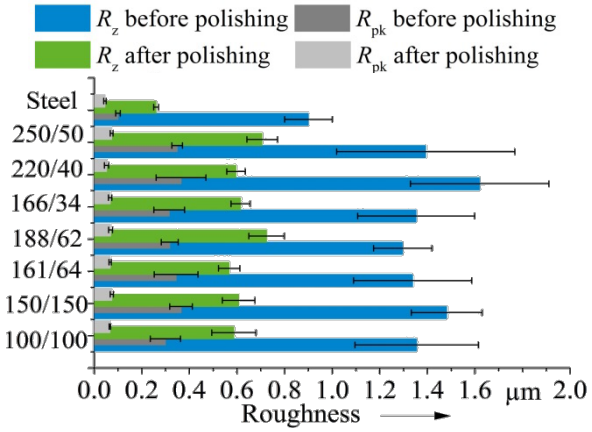

Fig. 7: Surface roughness of the coating samples before and after polishing

To quantify the strength of the deposition parameters and clarify the correlation between deposition parameters and coating properties the main effect size of each varied deposition parameter on coating properties was determined. Main effect plots [21] of acetylene to argon ratio on coating properties were shown in Fig. 8. The effect size implies that each factor affects the responses in a different way. As shown in Fig. 8 ratio if the coatings were deposited under 300 sccm gas flows. The C-H radicals attach more quickly to substrate boundary surface than the other atoms in the reactor [22]. Therefore higher concentration of C_2H_2 accelerates coating growth process by forming coating clusters more quickly. It was observed, that the deposition rate under 200 sccm was very low and almost not affect by gas compositions was observed. Due to low total flows or low pressure in the PECVD reactor, the gases were discharged with lower current. The ions and radicals in this plasma field gained not enough kinetic energy which was unbeneficial for coating growth. The resulting adhesion depends strongly on total gas amounts. Considering the high standard deviation, hardness and indentation modulus of the coatings are not very pronounced. As shown in Fig. 9, the deposition rate increases with the total process gas amount. The formation of clusters is precondition for the further growth steps [23]. The higher amount of total gas atoms in the reactor accelerates the growth of clusters and thus the formation of coatings. This effect is stronger if the C_2H_2 / Ar = 1:1. The a-C:H coating deposited under higher process pressure has generally better adhesion. If the C_2H_2 / Ar = 1:1 this effect is not very pronounced. However, hardness and indentation modulus decrease with raising gas amounts.

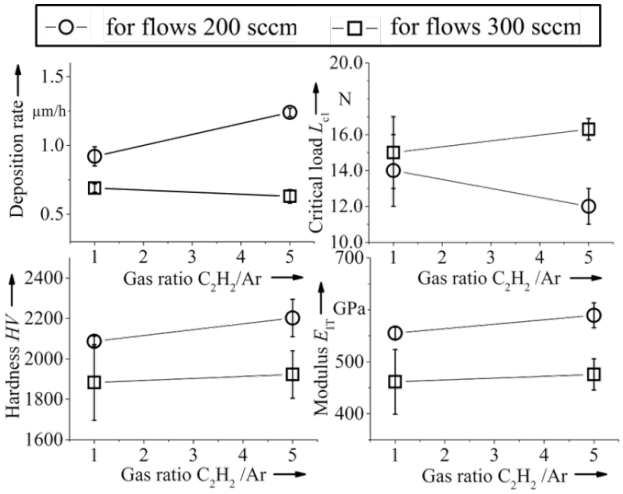

Fig. 8: Main effect size of acetylene to argon ratio on deposition rate, critical load of the first crack L_{c1}, Vickers hardness HV and indentation modulus E_{IT}, respectively.

According to Pujada et al. [24], the increasing C_2H_2 flow led to a reduction of hardness and indentation modulus in the WC doped a-C:H-matrix, as the C_2H_2 amount varied from 0 to 10 sccm. The investigation of [25] shows the same tendency, as the C_2H_2 amount varied from 7 to 49 sccm.

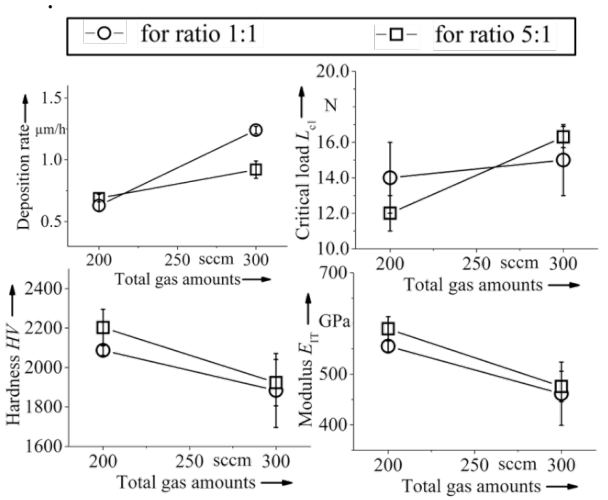

Fig. 9: Main effect size of total gas flows on coating deposition rate, critical load of the first crack L_{c1}, Vickers hardness HV and indentation modulus E_{IT}, respectively.

In the plasma with low total gas amounts the mean free path of each molecule is longer and thus lead to less energy loss through collision with other species. Ions with high energy promote the formation of sp^3 bonds [26] which is well known to be associated with high hardness and modulus. This statement fits reasonably for sp^3 rich and hardest amorphous carbon coating like ta-C, but less for a-C:H [27]. In the case of a-C:H coatings the hardness and modulus depend also on the form of the existing sp^2 bonded carbon atoms

which will be discussed with help of Raman data in the next passage.

Fig. 10 shows Raman spectra of all a-C:H coatings. The mainly investigated peaks are D peak and G peak, which lie at about 1560 cm^{-1} and 1360 cm^{-1}, respectively, for excitation using visible laser. Both of them describe states of sp^2-bonds. Because the excitation resonates with π states due to its lowest excitation energy. The G peak has its origin in bond stretching of all pairs of sp^2 hybridised carbon atoms in both rings and chains. The D peak describes the breathing modes of sp^2 hybridised atoms in rings.

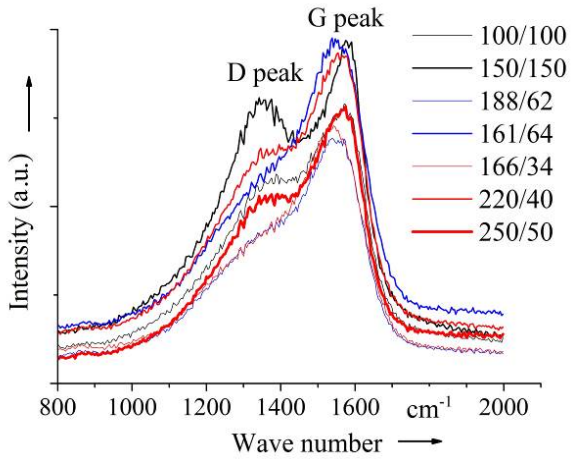

Fig. 10: Raman spectra of all a-C:H coatings using 532 nm Nd:YAG-laser.

A Raman spectrum is associated with clustering of the sp^2 phase, presence of sp^2 rings or chains and the sp^2/sp^3 ratio [28]. The intensity ratio I_D/I_G indicates the disorder level and the sp^3-content in the amorphous graphite phase for the DLC coating, which is also associated to the coating hardness [27]. The peak intensity is fitted by a Breit-Wigner-Fano (BWF) line for the G peak and a Lorentzian line for the D peak. The BWF + Lorentzian line pair were selected for curve fitting because they are well known for excellent fitting of Raman spectra for all carbons, from graphite to ta-C [29]. The calculation of I_D/I_G peak intensity ratios in this work was conducted using the software MatLab. The essential results of a-C:H coatings are summarized in Tab. 4.

Tab. 4: Raman parameters of all a-C:H variations.

C_2H_2/Ar / C_2H_2+Ar	1:1	3:1	5:1
200 sccm	Coating 100/100 I_D/I_G = 0.60 $FWHM_G$ = 155.0	Coating 161/64 I_D/I_G = 0.25 $FWHM_G$ = 198.9	Coating 166/34 I_D/I_G = 0.23 $FWHM_G$ = 204.7
250 sccm	-	Coating 188/62 I_D/I_G = 0.34 $FWHM_G$ = 184.9	Coating 220/40 I_D/I_G = 0.44 $FWHM_G$ = 171.7
300 sccm	Coating 150/150 I_D/I_G = 0.81 $FWHM_G$ = 124.2	-	Coating 250/50 I_D/I_G = 0.50 $FWHM_G$ = 155.4

Ferrari et al. [27], [29] had developed a three-stage model to describe different amorphization states with increasing disorder of sp^2 hybridised bonds. A G position from 1 571 to 1 592 cm^{-1} implies that all samples in this work can be considered as a mixture of nanocrystalline graphite and amorphous carbon network in both ring and chain configurations. According to [29], the sp^3 configuration increases from 0-20 % as the I_D/I_G decreases from 2.0 to 0.25. As shown in Tab. 4 the coatings had generally a sp^3 content of about 10-20 %. The precursor gas HC≡CH with triple bonds tends to form unsaturated :C─H radicals during deposition process. For formation of sp^3-bonds (C-H sigma bonds) additional hydrogen is required.

Relationships between the Raman parameters and mechanical properties were investigated. The configuration of chain is used to estimate the presence of sp^3 bonds. Higher sp^3 content is usually associated with higher hardness. As mentioned in the last passage, a smaller I_D/I_G implies presence of more sp^3 content. In Fig. 11 the coating hardness and indentation modulus decrease with increasing I_D/I_G due to less sp^3 bonds. According to [30], the FWHM of the G peak and the sp^2 grain size have a logarithms proportional relationship. The higher the FWHM values of G peak, the finer the sp^2 grain size. As mentioned before, the a-C:H coatings series can be described as a carbon network with large amount of small sp^2 clusters distributed in amorphous carbon network.

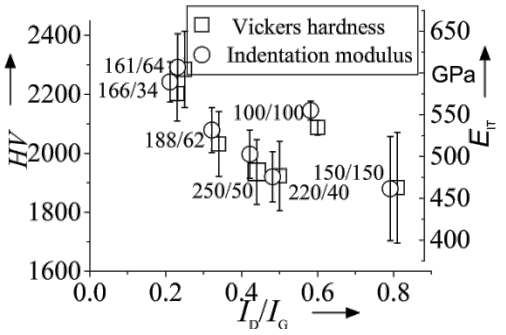

Fig. 11: Variation of Vickers hardness HV and indentation modulus E_{IT} with increasing I_D/I_G

In this paper, all involved a-C:H variations contain sp^3 content up to ≈ 20%. The grain size of sp^2 content is the second key parameter to estimate the coating hardness. According to the grain boundary strengthening theory (also called Hall-Petch Strengthening), the critical shear strength τ is inversely proportional to grain diameter D: $\tau \propto D^{-1/2}$ [Bay]. This explains in the aspect of material structure the high hardness of coating 166/34 and 161/64 as shown in Fig. 12. Because they exhibit sp^2 grains with finer size than the other coatings.

As can be seen, the deposition parameters affect strongly the coating properties like the deposition rate, interfacial adhesion, hardness and indentation modulus. The deposition rate increases with total gas flow due to formation of more clusters in the initial phase of the coating growth. The effect of gas flow ratio on deposition rate depends on process gas pressure: for processes with 200 sccm the effect of gas ratio was not very pronounced; for processes with 300 sccm the tendency is proportional. The effect size of gas ratio on

interfacial adhesion was also pressure dependent. Due to less energetic particles caused by short mean free path lengths in the plasma, hardness und indentation moduli reduce as the total gas flow rises and C2H2 concentration decreases.

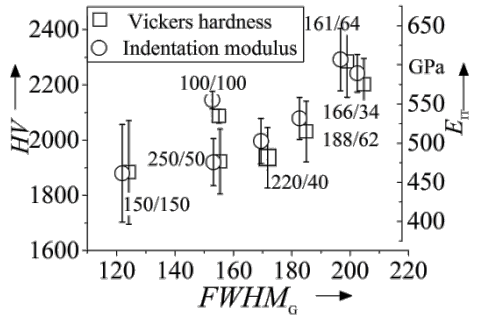

Fig. 12: Variation of Vickers hardness HV and indentation modulus E_{IT} with increasing FWHM of G peak

Raman spectra of all coatings samples show characteristic parameter to identify chemical bonds in the coating samples. All investigated coating samples can be described as a mixture of nanocrystalline graphite and a-C:H carbon network. Furthermore, the Raman parameters indicate that the sp3 content and sp2 grain sizes are two key parameters to determine their differences in hardness and modulus. Coating with lower ID/IG and higher FWHM of G peak is associated with more sp3 configuration and finer sp2 grain size and thus high hardness.

Fig. 12 reveals the effect sizes of deposition parameters on the two essential Raman parameters, which are associated with sp2 and sp3 configurations. As can be seen in the Fig. 13, a high C2H2/Ar ratio and low total gas amounts lead to smaller ID/IG intensity ratio and higher FWHM of G peak, which is associated with high hardness.

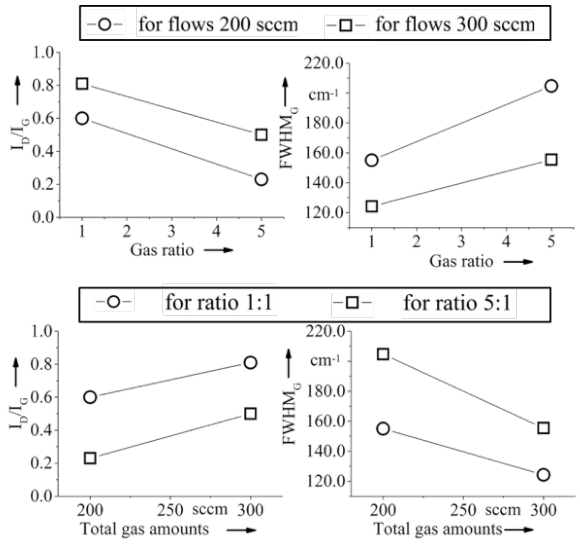

Fig. 13: Main effect size of gas flow ratios of C_2H_2/Ar and total gas amounts on the Raman parameters I_D/I_G and $FWHM_G$

3.2 ta-C coating

The tetrahedral hydrogen free amorphous carbon coating system (ta-C) consists of an Cr adhesive layer and the ta-C functional layer. For a smooth coating surface the Cr adhesive layer of about 600 nm was generated by sputtering. The ta-C coating of about 700 nm was manufactured by laser cathodic vacuum arc process. The arc process was initiated by a laser pulse on the graphite target [32]. In order to ensure a smooth coating, a magnetic field was applied to remove the macroparticles during coating deposition. After the deposition the coated specimens were mechanically treated by polishing and brushing with diamond paste with a grain size of 3 µm. The coating properties are summarized in Tab. 5.

Tab. 5: Coating characterizations of ta-C coating

t in µm	L_{c1} in N	HV0.001	E_{IT} in GPa	R_z in µm	R_{pk} in µm
1.33 ± 0.03	12.0	3 827±599	331 ± 52	0.26 ± 0.01	0.045 ± 0.005

3.3 Laser based graphitization of ta-C coating

To investigate the tribological behavior of a ta-C coating with varying sp^2/sp^3 ratios the ta-C coating was locally graphitized by means of laser heat treatment. For this purpose, the range of the ta-C coating dependent energy input which is necessary for graphitization was experimentally evaluated by the zero-damage method of line-shaped features [33]. The energy range is enclosed by the graphitization threshold as the lower limit and the ablation threshold as the upper limit of the applied laser fluence F. An ultrashort pulsed laser system (Fuego, Time-Bandwidth Products) with pulse duration $\tau = 10$ ps was applied for graphitization and later for micro feature generation. Usually, ultrashort laser pulses induce cold material ablation and thus, offer the possibility to generate micro features with minimal heat affected zones. However, aiming at an efficient heat treatment and graphitization, a high pulse frequency $f_P = 1.0$ MHz at a low scanning speed $v_S = 50$ mm/s were used to enable strong heat accumulation. Due to a low spatial pulse-to-pulse-distance $p_x = 0.05$ µm with a spot diameter $d_0 = 50$ µm the succeeding laser pulses lead to a temperature rise. To realize a tailored heat input the laser wavelengths $\lambda_1 = 1064$ nm and $\lambda_2 = 355$ nm were investigated. Although the ta-C layer is transparent in the near-infrared wavelength range, the laser based graphitization should be possible at wavelength λ_1 due to multi-photon absorption. In contrast, heat input by processing at wavelength λ_2 occurs due to linear absorption as the bandgap of a similar ta-C coating with an sp^3-fraction of 80% is $E_G = 2.6$ eV which corresponds to the wavelength $\lambda_G = 477$ nm [34]. These admissions are confirmed by the evaluated wavelength dependent graphitization and ablation thresholds (Fig. 14). As it is depicted in Fig. 14 the thresholds for $\lambda_1 = 1064$ nm are higher than for $\lambda_2 = 355$ nm due to necessary multi-photon absorption with minimum three photons to exceed the bandgap.

For the generation of two-dimensional surface graphitization areas of 200 µm x 500 µm were laser irradiated. The topography of four of these areas is exemplarily shown in Fig. 14.

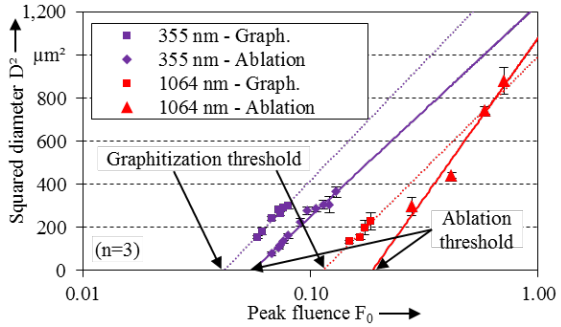

Fig. 14: Measured widths of line-shaped features depending on the wavelength and the peak fluence to determine the graphitization and ablation thresholds

Processing at $\lambda_2 = 355$ nm enables homogenous graphitization without any changes of the surface roughness which does not depend on the applied peak fluence (Tab. 6). In contrast, the low increase of the peak fluence in processing at $\lambda_1 = 1064$ nm leads to the doubling of the roughness due to local removal of the layer respectively laser induced craters (Fig. 15b).

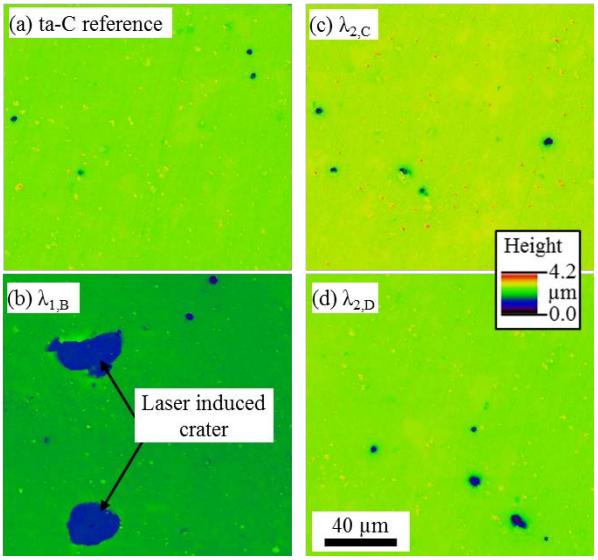

Fig. 15: Topography of graphitized areas which were laser treated at (a) $\lambda_1 = 1064$ nm and (b-d) $\lambda_2 = 355$ nm

These craters are probably induced by the ablation of Cr particles in the ta-C coating as Cr is used as additional adhesive layer. The ablation threshold of Cr is lower than the ablation threshold of the ta-C coating itself, thus resulting in the observed damages of the coating. Thus, laser treatment at $\lambda_1 = 1064$ nm leads to rough areas (Tab. 6).

Tab. 6: Mean average roughness *Sa*, reduced peak height *Spk* and maximum height *Sz* of graphitized areas laser treated at $\lambda_1 = 1064$ nm and $\lambda_2 = 355$ nm (n = 3)

Sample	F_0 in J/cm²	*Sa* in µm	*Spk* in µm	*Sz* in µm
ta-C Ref.	-	0.03 ± 0.01	0.07 ± 0.01	2.65 ± 0.04
$\lambda_{1,A}$	0.029	0.03 ± 0.01	0.08 ± 0.01	3.10 ± 0.04
$\lambda_{1,B}$	0.031	0.06 ± 0.02	0.20 ± 0.12	5.38 ± 0.19
$\lambda_{2,C}$	0.076	0.03 ± 0.01	0.06 ± 0.01	2.30 ± 0.02
$\lambda_{2,D}$	0.079	0.03 ± 0.01	0.07 ± 0.01	2.64 ± 0.21

Micro hardness measurements of seven chosen areas which were laser treated with different peak fluences at $\lambda_2 = 355$ nm reveal a slight decrease of hardness of the ta-C coating hardness due to graphitization (Fig. 16). The indentation hardness H_{IT} as well as the indentation modulus E_{IT} slightly decrease with higher fluence respectively heat input, although the results are within the deviation. The applied peak fluences $F_{0,5}$ to $F_{0,7}$ result in mechanical parameters, which are significantly lower than the untreated ta-C reference.

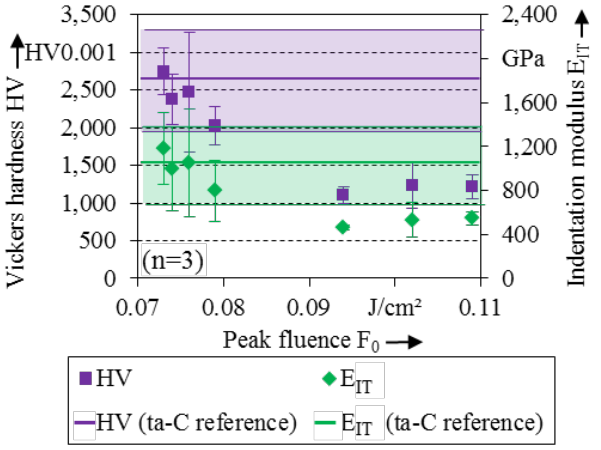

Fig. 16: Vickers hardness *HV 0.001* and indentation modulus E_{IT} depending on the peak fluence F_0 which was applied for laser based graphitization at $\lambda_2 = 355$ nm

The variation of the mechanical properties is caused by structural changes of the treated coating. The analysis by Raman spectroscopy reveals I_D/I_G-ratios and FHWMs of the G-peak which are rising with higher peak fluence due to higher heat input (Fig. 17). The I_D/I_G-ratio of the untreated reference is about 0.06 ± 0.01 and the spectrum of the reference shows one broad peak resulting from the D- and G-peak (Fig. 17b) and c)) [29]. Heat input by laser treatment leads to splitting of both peaks (Fig. 17c)), smaller D- and G-peaks (Fig. 17 b)) as well as a rising I_D/I_G-ratio up to 0.55 ± 0.13 at the peak fluence $F_0 = 0.076$ J/cm² due to an increase of the D-peak. An increasing D-peak indicates graphitization of the coating [29].

Correspondingly, ultrashort pulsed laser graphitization enables the adjustment of structural as well as mechanical properties of ta-C coatings without any changes of the surface topography in the micrometer range. The effects on the tribological behavior of ta-C coatings are discussed in chapter 4.2. As the range of energy input of laser based heat treatment at $\lambda_1 = 1064$ nm is limited due to rising roughness of the coating surface the homogenous and more significant graphitization has to be an object in future investigation steps. To extend the range of laser based heat treatment a top-hat intensity profile instead of the used Gaussian profile of the laser beam represents an appropriate approach.

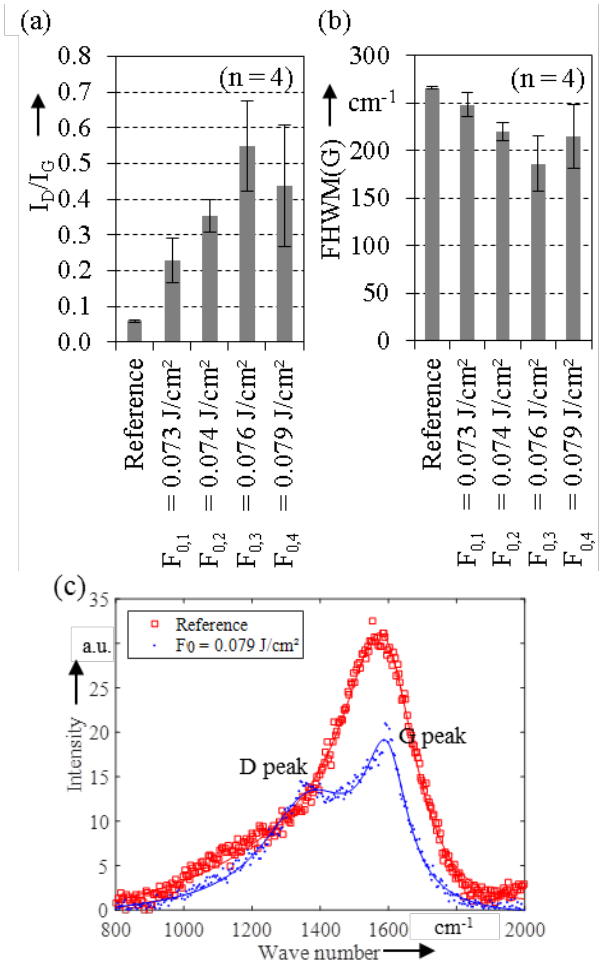

Fig. 17: (a) I_D/I_G-ratio and (b) FHWM of the G-peak of the taC coating reference and laser irradiated areas (λ_2 = 355 nm) as well as (c) exemplary Raman spectra of the reference and the area which was irradiated by peak fluence $F_{0,4}$ = 0.72 J/cm²

3.4 Laser based texturing of ta-C coating

To control the material flow and decrease fluctuations of the friction coefficient [35], laser generated micro features were introduced into the original ta-C coating type. The material removal was realized at λ_1 = 1064 nm. To avoid heat accumulation and thus, heat affected zones a low pulse frequency f_P = 50 kHz was applied. Each of the micro features has the same lateral dimension at the surface of width W = 500 µm and length L = 200 µm parallel to the sliding direction. The generated features have to be distinguished concerning the feature depth which is $d_1 \approx 0.5$ µm for the flat and $d_2 \approx 5$ µm for the deep configuration (Fig. 18).

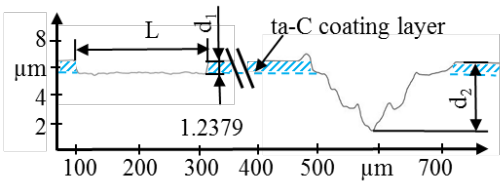

Fig. 18: Measured cross sections of the generated micro features with depth d_1 = 0.5 µm and $d_2 \approx 5$ µm

The ta-C coating layer is removed by parameter setting A for each feature. Additionally, for the deep features the material ablation of 1.2379 is generated by the additional parameter set B (Tab. 7).

Tab. 7: Parameter settings of successive laser texturing steps for micro feature generation with low (A) and high (A+B) feature depth. The scanning speed for each set was 68 mm/s

Step No.	Peak fluence F_0 in J/cm²	Spot diameter d in µm	Hatch distance p_y in µm	Number of passes N
A	1.0	80	30	1
B	3.0	32	10	4

4 Tribological behavior of coated tools

4.1 Tribological behavior of a-C:H coated tools

In Fig. 19 the friction coefficients μ_{rod} against two aluminium alloys (AA5182 and AA6014) of one coating variant 220/40 were shown over the sliding distance using ring-on-disc-tribometer. Fig. 19a) depicts the sliding behaviour of three repeated tests against AA5182. Due to close tribological system the different friction behaviours in the initial phase (s = 0.3-0.8 meter) and the late phase (s = 9-10 meter) were observed. In this case, the results in the late sliding phase can be affected by the previous wear status and flattening of the sheet surface. In the initial phase coatings 220/40 show friction plateaus with very low friction coefficients of about 0.25. This implies no adhesive friction occurred at the beginning of test. After the phase with plateau, aluminium adhesions started to propagate in a not repeatable way which results in an unstable and higher friction. As soon as the aluminium adhesions accumulated to a certain height, the a-C:H coating has no more or little contacts to aluminium alloy sheet. Fig. 19b) shows friction coefficient μ_{rod} of coating 220/40 against AA6014.

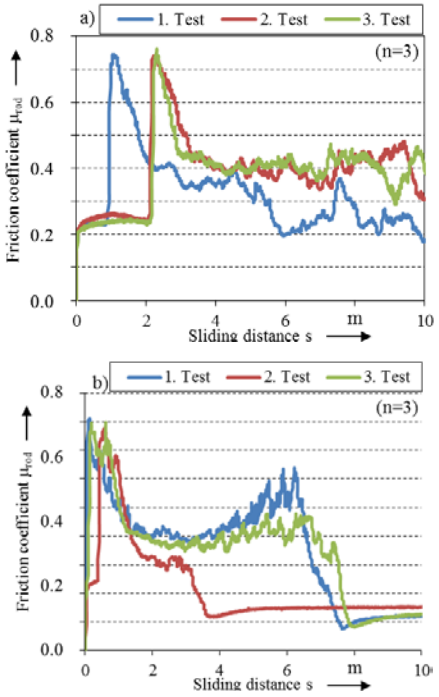

Fig. 19: The variation of the friction coefficient μ_{rod} of three repeats over sliding distance tested against a) AA5182 and b) AA6014 at contact pressure of 2.1 MPa

The coating 220/40 behaves differently in tests against AA6014. A short μ_{rod} plateau at the beginning of sliding was observed only in the second repeated test. The friction of other repeats tended to rise immediately to very high value at the beginning. Stable μ_{rod} after 4 or 8 m sliding distance was observed.

As mentioned before, the appearance of a plateau phase at the beginning of sliding is essential and beneficial for the real forming process. To characterize the appearance of steady plateaus, mean values of μ_{rod} from 0.3 to 0.8 meter are calculated and summarized in Fig. 20.

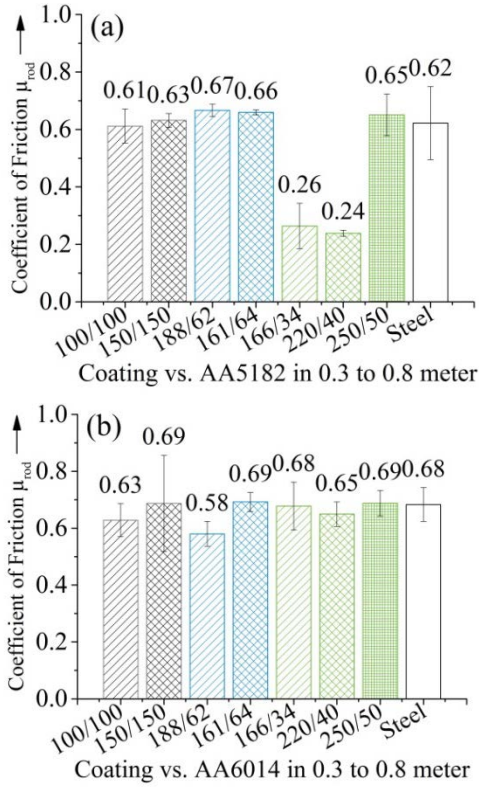

Fig. 20: Mean values of friction coefficient μ_{rod} (n=3) of all coatings within sliding distance from 0.3 to 0.8 m when tested against a) AA5182 and b) AA6014 at contact pressure of 2.1 MPa using ring-on-disc-tribometer

Coatings 166/34 and 220/40 against AA5182 show reliable and steady low μ_{rod} after three repetitions at the beginning of sliding. The results against AA6014 did not show a remarkable difference.

As depicted in Fig. 19, the low friction is often associated with appearance of a stable phase without aluminum transfer. In order to characterize the stable phase, the mean values of μ_{rod} from 9 to 10 meter are summarized in Fig. 21. It is noticeable, that friction coefficients of all coatings against AA5182 show high standard deviations due to adhesive friction. Besides coating 220/40, the coating 250/50 also shows particularly lower μ_{rod} against AA6014.

The worn surfaces were analysed by LSM. In Fig. 22 two examples against both aluminium alloys were shown. As depicted in Fig. 22, more aluminium adhesions were observed if sliding against AA5182. The adhesion on coating 188/62 against AA5182 was analysed with a height of about 2 µm. In addition, worn surfaces against AA6014 were observed with little to no visible adhesion. Large area of adhesion was observed on worn surface 150/150 against AA5182.

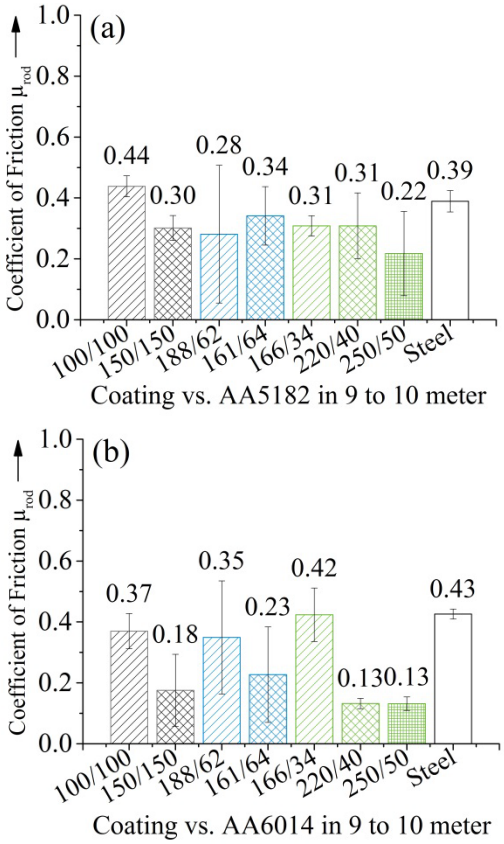

Fig. 21: Mean values of friction coefficient μ_{rod} (n=3) of all coatings within sliding distance from 9 to 10 meter when tested against a) AA5182 and b) AA6014 using ring-on-disc-tribometer

Thin aluminium adhesion film in outer ring area was observed for the worn surface 150/150 against AA6014.

In summary, the a-C:H coating variations behave differently in the simple ring-on-disc tribometer. Some of the coating variations show low μ_{rod} in initial phase and steady phase. Coatings deposited under high acetylene concentration are found to have a clear characteristic plateau with low μ_{rod} to about 0.2 against AA5182 in the initial phase of tribological test. The same plateaus were also observed against AA6014 only for a short sliding distance. Coatings with this μ_{rod}-plateau behave very beneficial in process-like strip drawing test.

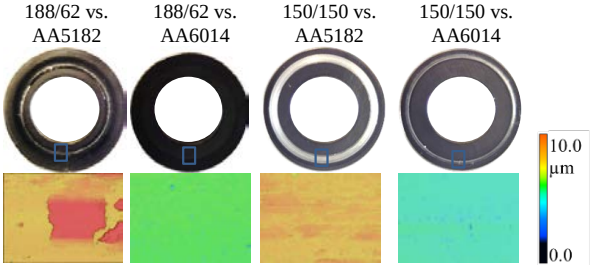

Fig. 22: Wear appearances of worn coating surfaces 188/62 and 150/150 against AA5182 and AA6014 measured by laser scanning microscope

The coatings with plateaus in initial phase are deposited under high C_2H_2/Ar ratio. No such plateau was observed for coating deposited under ratios of 1:1 and 3:1 from Fig. 20a). The Ar plasma bombarded the surface strongly during the deposition process, especially if the Ar-concentration was excessive. The high density ion bombardment contributes to increased numbers of the so-called adatoms as well as adsorption sites [20], [22], which may lead to weak bonds [36] or even loose atoms on surface. This makes the coating structure inhomogeneous or porous. Thus, those coatings take longer time to set the stabilized sliding state.

4.2 Tribological behavior of locally modified ta-C coated tools

To clearly derive the effect of a varied sp^2/sp^3 ratio the ta-C coating is partially graphitized. Thus, the coating has identical properties regarding thickness, adhesive layer and roughness. For the graphitization, wavelength λ_2 = 355 nm, pulse frequency f_P =1 MHz, peak fluence F_0 = 0.079 J/cm², scanning speed v_S = 50 mm/s and hatch distance p_y = 3 µm were applied to locally generate rectangular areas of width W = 500 µm and length L = 100 µm which cover δ_F = 50% of the ring surface. The ring-on-disc test of these rings in contact with zinc-coated DC04 sheets reveals a similar behaviour of the friction coefficient μ_{rod} at the beginning of sliding (Fig. 23). On the surfaces of the references as well as the graphitized rings a transfer film develops. In stationary sliding the higher amount of sp^2-hybridized carbon atoms on the graphitized rings leads to a significantly higher friction coefficient.

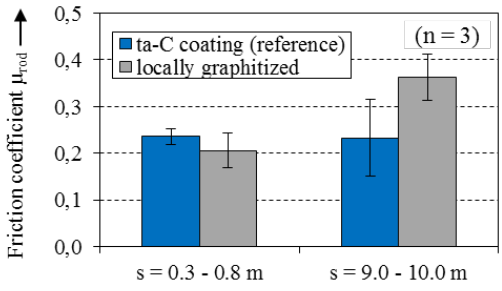

Fig. 23: Friction coefficient in running-in phase (s = 0.3-0.8 m) and at stationary sliding (s = 9.0-10.0 m) of untreated ta-C coating and laser based graphitized ta-C coating (λ_2 = 355 nm, F_0 = 0.72 J/cm², p_y = 3 µm; δ_F = 50%, W = 500 µm, L = 100 µm)

Despite of this higher friction the surface of the graphitized ring surfaces does not show any indications of increased wear compared to the reference rings (Fig. 24). Each of the ring surfaces shows an area of smoothened ta-C at the outer edge.

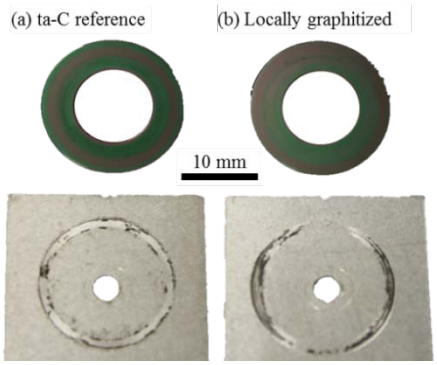

Fig. 24: Exemplary ta-C coated (a) and additionally laser heat treated (b) ring surfaces as well as zinc-coated DC04 sheets which were in contact for the total sliding distance s = 10.0 m

The thickness of the removed ta-C layer in this area is less than 50 nm. As the samples had the same topography prior to the ring-on-disc tests, the higher sp^2-fraction respectively lower hardness due to laser heat treatment induces increasing friction.

4.3 Tribological behavior of textured tools with ta-C coatings

The tribological mechanisms of textured tools strongly depend on the amount and distribution of adhesive and loose wear particles. Thus, analyzing the tribological properties of micro features in a closed system would strongly distort the results. Therefore, the friction coefficients determined in closed tribometer tests could not be transferred to the behavior in real forming processes. Hence, in this study the performance of ta-C coated tools with micro features is directly investigated in strip drawing tests. Roch et al. described a possible friction reduction of 30 % with textured ta-C tools in a tribometer test rig depending on geometry and orientation of the patterns under dry conditions [35]. As positive influence a reduce contact area and the possibility to trap wear debris within the patterns was described. Similar effects could be observed in the present investigation. Depending on the percentage coverage an approximately 20 % lower friction coefficient could be achieved with laser generated micro features. The combination of laser generated micro features with ta-C coatings was analyzed under process-like conditions in strip drawing tests in contact with DC04. The percentage friction in relation to tests with ta-C coated friction jaws without micro features is shown in Fig. 25. In order to evaluate the general tribological mechanisms of textured surfaces the percent of coverage and the depth of micro features was varied in two steps. Additionally, the applied normal force F_N was varied depending on the percentage coverage. One test series was performed with 4.5 MPa considering that the contact area was reduced due to micro features to 65 % and 50%, respectively. Afterwards, the tests were conducted with the normal force F_N referring to the nominal contact area of 100 mm x 55 mm. Thus, the "effective" contact pressure for the right-hand side bars varies from 6.9 MPa to 9 MPa depending on the level of coverage.

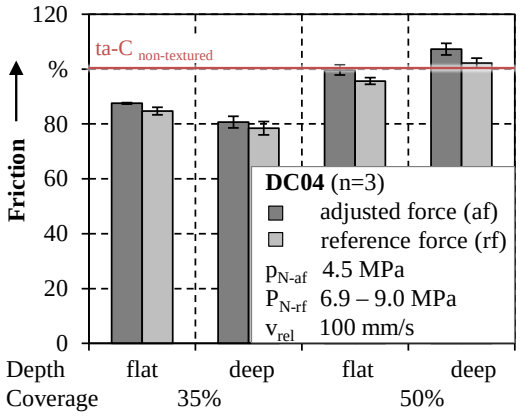

Fig. 25: Friction for ta-C coated and textured tools in strip drawing tests

For micro feature coverage of 35 % the friction could be reduced significantly for flat and deep configurations. In contrast, if half of the contact surface is covered with micro features the friction can slightly be reduced for flat textures and even increases for deep ones. The percentage coverage seems to have a greater influence compared to depth of features. Besides, for all tests a slight friction decrease is caused by increase of contact pressure. For the tests with 50 % coverage the contact pressure was doubled comparing the left and right bars in Fig. 25. Thus, the difference between the two levels of contact pressure is higher than for tests with 35 % coverage. There is no distinct influence of flat and deep configurations because of their reverse behavior for the two levels of coverage. Different tribological mechanisms seem to determine the friction and wear behavior for textured surfaces. On the one hand side, micro features decrease the real contact area which leads to increased contact pressure. This causes a stronger flattening of the sheet surface which reduces the resistance against sliding. On the other hand side, micro features lead to less roughness asperities which are in direct contact. Therefore, micro features are beneficial to reduce interlocking of single asperities. Both, a decreasing contact area and less interlocking lead to lower friction. In contrast, micro features might evoke an increase of abrasion due to shearing of roughness peaks at the feature edges. In this investigation the percentage coverage is adjusted by the number of micro features and not by their size. Thus, higher percentage coverage means also an increasing amount of features. With a higher number of features the effect of shearing on feature edges is increased. There seems to be a turning point around or slightly below 50 % coverage at which the influence of shearing asperities at feature edges becomes dominant for the investigated topographies. The contact conditions at beginning of strip drawing tests are exemplarily visualized in Fig. 26. In order to depict tool and workpiece surface in direct contact the measured P-profile for DC04 was turned 180°. At first, only some roughness asperities will have direct contact which leads to locally increased contact pressure. A higher pressure at the contacting asperities will cause flattening of the softer contact partner – in this case DC04. Thus, more roughness peaks will get in contact. Depending on the depth of laser generated textures it might be possible that some roughness peaks even contact the bottom of the features. Therefore, it seems reasonable that the deep configuration at a coverage of 35 % lead to lower friction than the flat features.

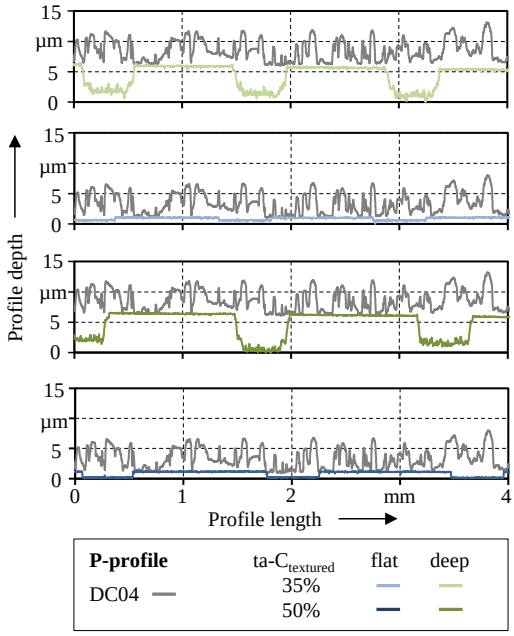

Fig. 26: P-profile for DC04 in contact with ta-C coated and textured surfaces

In order to understand why at 50 % coverage the deeper features caused a higher friction a surface analysis was performed. The results are shown in Fig. 27. The abrasive effect due to shearing of asperities on features edges could be observed for deep textures with 50 % coverage. This interlocking and abrasion of zinc particles increase the resistance against sliding and cause higher friction. Thus, for future investigations it might be beneficial to create smoother feature edges.

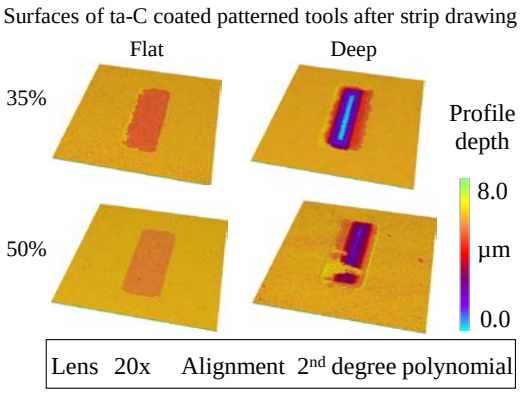

Fig. 27: Tool topographies after strip drawing tests

5 Summary and Outlook

In the current study the tailored modification of carbon based coatings for the tool-sided application in dry deep drawing processes was analyzed. Due to diverse predominating tribological mechanisms for aluminum alloys and deep drawing steel different modifications were developed depending on the sheet

material. A summary of the main results achieved with different modification approaches and the next steps is given in Fig. 28.

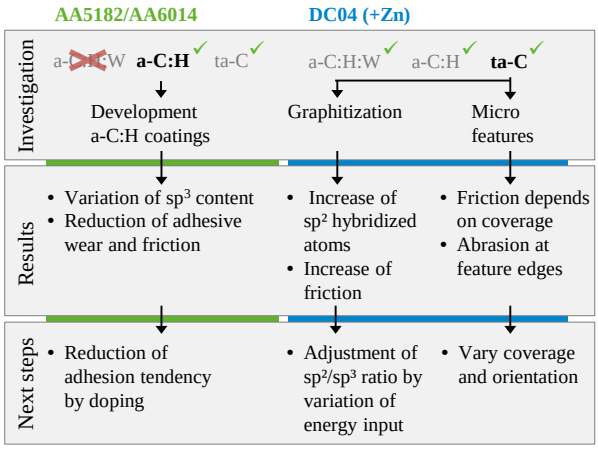

Fig. 28: Summary and next steps

The relationships between coating deposition parameters, coating properties and tribological behavior were investigated for a-C:H coatings in contact with aluminum alloys. Especially, the total gas flow/pressure seems to have a significant influence on coating properties. A higher total gas flow leads to higher deposition rate and adhesion but lower hardness and modulus. Regarding the tribological properties, coatings deposited at high C_2H_2/Ar ratio revealed friction plateaus at the initial phase against AA5182. The same coating groups are found to have a low and stable friction against AA6014 in the stationary phase. The wear surfaces against AA6014 were found to have less adhesion than that against AA5182. This leads to a stationary friction of some a-C:H coatings against AA6014 from 4 to 8 meter. In future investigations promising a-C:H variants will be deposited on friction jaws in order to proof if the beneficial behavior occurs as well in an open tribological system.

In order to realize a broad range of friction coefficients for the local control of the material flow, laser based modifications of ta-C coatings were evaluated. In this study a process window regarding the ultrashort pulsed laser based processing parameters for graphitization of ta-C coatings was developed. The laser based heat treatment of ta-C coatings caused increasing friction after the running-in phase compared to untreated ta-C coatings in ring-on-disc tests of zinc-coated DC04 sheets. Thus, it was proofed that increasing sp^2 content leads to higher friction. A laser based heat treatment of carbon based coatings seems a promising approach to locally adapt friction. Further studies will examine the effect of different ratios of graphitization regarding the tribological behavior in the ring-on-disc tests. In a next step, the transferability of the tribological behavior to strip drawing tests will be investigated. The graphitization will be varied by the laser based heat input.

Besides graphitization, micro features are a promising approach to locally vary the level of friction depending on the percentage coverage. In tribological tests with DC04, textured ta-C tools could achieve up to 20 % lower friction. The influence of the micro features depends on feature depth and percentage coverage. Patterned surfaces cause locally increased contact pressure due to a smaller real contact area. This results in increased flattening of the sheet surface which seems beneficial for the tribological behavior. Furthermore, micro features lead to less interlocking of roughness asperities because there is a reduced direct contact of tool and workpiece roughness peaks. Besides these positive mechanisms, micro features evoke shearing of asperities on feature edges. Depending on the percentage coverage, this effect becomes dominant and thus leads to increasing friction as shown for 50 % coverage. Future investigations with further levels of percentage coverage will be performed to find a compromise between reduced real contact area and shearing of asperities. Furthermore, applying textured ta-C tools in contact with aluminum alloys will be analyzed. Due to different topography with higher amount of single roughness asperities and increased adhesion tendency of aluminum alloys the results will not be directly transferable. Thus, future studies will show if the same processing parameters can be applied for different sheet materials.

Acknowledgement

The authors thank the German Research Foundation (DFG) for supporting the presented investigations by funding the priority program SPP 1676 project ME 2043/43-1, SCHM 2115/36-1 and TR 1043/1-1 with the project title “Lubricant free forming with tailored tribological conditions”.

References

[1] F. Vollertsen, F. Schmidt: Dry Metal Forming: Definition, Chances and Challenges. International Journal of Precision Engineering and Manufacturing - Green Technology 1(1) (2014) 59-62

[2] N. Bay, A. Azushima, P. Groche, I. Ishibashi, M. Merklein, M. Morishita, T. Nakamura, S. Schmid, M. Yoshid: Environmentally benign tribo-systems for metal forming. CIRP Annals - Manufacturing Technology 59(2) (2010) 760–780

[3] T. Mang, W. Dresel: Lubricants and Lubrication. 2nd Ed., John Wiley and Sons (2007)

[4] Association of German Engineers (VDI): VDI Guideline 2840. Beuth (2012)

[5] J. Steiner, R. Zhao, S. Tremmel, M. Merklein: Investigation of Tribological Behavior of Carbon Coatings in Dry Sheet Metal Froming. In: K. Bobzin, K.-D. Bouzakis, B. Denkena, H. J. Maier, M. Merklein (Hrsg.): The "A" Coatings Conference Proceedings PZH Verlag (2016) 153-160

[6] J. Vetter: 60 years of DLC coatings: Historical highlights and technical review of cathodic arc processes to synthesize various DLC types, and their evolution for industrial applications. Surface and Coating Technology 257 (2014) 213-240

[7] M. Merklein, M. Schmidt, S. Wartzack, S. Tremmel, K. Andreas, T. Häfner, R. Zhao, J. Steiner: Development and Evaluation of Tool Sided Surface Modifications for Dry Deep Drawing of Steel and Aluminum Alloys. Dry Metal Forming Open Access Journal (2015) 121-133

[8] T. Mang, K. Bobzin, T. Bartels: Industrial Tribology. Wiley-VCH Verlag GmbH & Co. KGaA (2011)

[9] German Institute for Standardization (DIN): DIN EN ISO 4287. Beuth (2010)

[10] German Institute for Standardization (DIN): DIN EN 1071. Beuth (2003)

[11] German Institute for Standardization (DIN): DIN EN ISO 14577. Beuth (2003)

[12] A.C. Ferrari, J. Robertson: Raman spectroscopy of amorphous, nanostructured, diamond-like carbon, and nanodiamond. Philosophical Transactions of the Royal Society of London A 362 (2004) 2477-2512.

[13] S. Prawer, K.W. Nugent, Y. Lifshitz, G.D. Lempert, E. Grossman, J. Kulik, I. Avigal, R. Kalish: Systematic variation of the Raman spectra of DLC films as a function of sp2:sp3 composition. Diamond and Related Materials 5(3-5) (1996) 433-438.

[14] R. Zhao, S. Tremmel: PVD-/PECVD-DLC Thin Coatings as a Potential Solution for Tailored Friction Conditions for Dry Sheet Metal Forming Tools. Proceedings of the 12th THE A Coating (2016) 193-200

[15] J. Wang, Z. Cao, F. Pan, F. Wang, A. Liang, J. Zhang, Tuning of the microstructure, mechanical and tribological properties of a-C:H films by bias voltage of high frequency unipolar pulse, Applied Surface Science. 356 (2015) 695-700.

[16] Y. Pauleau, Residual Stresses in DLC Films and Adhesion to Various Substrates. In: C. Donnet, A. Erdemir, Tribology of Diamond Like Carbon Films. Springer, New York, 2008.

[17] N.M.S. Marinsa, R.P. Mota, R.Y. Honda, P.A.P. Nascente, M.E. Kayama, K.G. Kostov, M.A. Algatti, N.C. Cruz, E.C. Rangel, Properties of hydrogenated amorphous carbon films deposited by PECVD and modified by SF6 plasma, Surface and Coatings Technology, 206 (2011) 640-645.

[18] S. Sattel, J. Robertson, H. Ehrhardt, Effects of deposition temperature on the properties of hydrogenated tetrahedral amorphous carbon, Journal of Applied Physics. 82 (1997) 4566-4576.

[19] A. N. Fadzilah, M. Rusop: Effect of deposition temperature of amorphous carbon thin films, in: International Conference on Electronic Devices, Systems and Applications (ICEDSA), Kuala Lumpur, Malaysia, 2011, 328-332.

[20] G. Capote, G.C. Mastrapa, V.J. Trava Airoldi: Influence of acetylene precursor diluted with argon on the microstructure and the mechanical and tribological properties of a C:H films deposited via the modified pulsed DC PECVD method. Surface and Coating Technology 284 (2015) 145-152

[21] W. Kleppmann: Taschenbuch Versuchsplanung. Produkte und Prozesse optimieren. 7th ed. Hanzer (2011)

[22] J. Robertson: Diamond like amorphous carbon. Material Science Engineering Review. 37(4-6) (2002) 129-281

[23] B. Rother, J. Vetter: Plasma-Beschichtungsverfahren und Hartstoffschichten. deutscher Verlag für Grundstoffindustrie (1992)

[24] B.R. Pujada, G.C.A.M. Janssen: Density, stress, hardness and reduced Young´s modulus of W-C:H coatings. Surface and Coating Technology 201 (2006) 4284-4288

[25] H. Hetzner: Systematische Entwicklung amorpher Kohlenstoffschichten unter Berücksichtigung der Anforderungen der Blechmassivumformung. Dissertation (2014)

[26] H.-G. Fuss, M. Frank: Industrial Production of DLC Coatings. In: C. Donnet, A. Erdemir: Tribology of Diamond-Like Carbon Films. Springer (2008)

[27] A. C. Ferrari, J. Robertson: Resonant Raman spectroscopy of disordered amorphous, and diamond-like carbon. Physical Review B. 64(7) (2001) 075414.

[28] M. Rigolio, C. Castiglioni, G. Zerbi, F. Negri: Density functional theory prediction of the vibrational spectra of polycyclic aromatic hydrocarbons: effect of molecular symmetry and size on Raman intensities. Journal of Molecular Structure 563-564 (2001) 79-87.

[29] A.C. Ferrari, J. Robertson: Interpretation of Raman spectra of disordered and amorphous carbon. Physical Review B, 61 (2000) 14095-14107

[30] A. C. Ferrari, S. E. Rodil, J. Robertson: Interpretation of infrared and Raman spectra of amorphous carbon nitrides. Physical Review B 67 (2003) 155306.

[31] G. Gottstein: Materialwissenschaft und Werkstofftechnik, Physikalische Grundlagen. 4th. ed. Springer Vieweg (2014) 266-268.

[32] T. Stucky, U. Baier, C.-F. Meyer, H.-J. Scheibe, B. Schultrich: Großflächenbeschichtung mit superhartem Kohlenstoff. Vakuum in Forschung und Praxis 6 (2003)

[33] J.M. Liu: Simple Technique for Measurements of Pulsed Gaussian-beam Spot Sizes. Opt. Lett. 7(5) (1982) 196-198

[34] B.K. Tay, X. Shi, E. Liu, H.S. Tan, L.K.Cheah, J. Shi, E.C. Lim, H.Y. Lee: Tribological and optical properties of hydrogen-free Amorphous Carbon Films with Varying sp^3/sp^2Composition. Surace and Interface Analysis 28 (1999) 226-230

[35] T. Roch, V. Weihnacht, H.-J. Scheibe, A. Roch, A.F. Lasagni: Direct Laser Interference Patterning of tetrahedral amorphous carbon films for tribological applications. Diamond & Related Materials 33 (2013) 20-26

[36] K. Bobzin: Oberflächentechnik für den Maschinenbau. 1st ed. Wiley-VCH Verlag (2013)